Structure vs Chemistry: Friction and Wear of Pt-Based Metallic Surfaces

ARTICLE *in* ACS APPLIED MATERIALS & INTERFACES · NOVEMBER 2013

Impact Factor: 6.72 · DOI: 10.1021/am403564a · Source: PubMed

3 AUTHORS, INCLUDING:

Arnaud Caron

Korea University of Technology and Education

38 PUBLICATIONS **283** CITATIONS

SEE PROFILE

ACS APPLIED MATERIALS & INTERFACES

Research Article

www.acsami.org

Structure vs Chemistry: Friction and Wear of Pt-Based Metallic Surfaces

A. Caron,*[,†] D. V. Louzguine-Luzguin,[‡] and R. Bennewitz[†]

[†]INM − Leibniz-Institute for New Materials, Nanotribology Group, Campus D2 2, 66123 Saarbrücken, Germany

[‡]WPI-Advanced Institute of Materials Research, 2-1-1 Katahira Aoba-ku, Sendai 980-8577, Japan

ABSTRACT: In comparison of a $Pt_{57.5}Cu_{14.7}Ni_{5.3}P_{22.5}$ metallic glass with a Pt(111) single crystal we find that wearless friction is determined by chemistry through bond formation alloying, while wear is determined by structure through plasticity mechanisms. In the wearless regime, friction is affected by the chemical composition of the counter body and involves the formation of a liquid-like neck and interfacial alloying. The wear behavior of Pt-based metallic surfaces is determined by their structural properties and corresponding mechanisms for plastic deformation. In the case of Pt(111) wear occurs by dislocation-mediated homogeneous plastic deformation. In contrast the wear of $Pt_{57.5}Cu_{14.7}Ni_{5.3}P_{22.5}$ metallic glass occurs through localized plastic deformation in shear bands that merge together in a single shear zone above a critical load and corresponds to the shear softening of metallic glasses. These results open a new route in the control of friction and wear of metals and are relevant for the development of self-lubricated and wear-resistant mechanical devices.

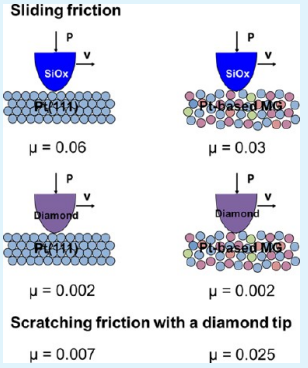

KEYWORDS: *metals, amorphous metals, friction, wear, AFM, FFM, ultrahigh vacuum*

I. INTRODUCTION

The effectiveness and durability of mechanical devices involving sliding contact are limited by friction loss and wear rate. For such applications metals are still the most relevant materials. Among metallic materials metallic glasses constitute a relatively new class of materials with promising properties, such as high surface quality with low roughness, low elasticity modulus, high yield strength, and hardness, for their applications as wear-resistant thin films, protective coatings, or microscale devices.

Two models have so far been available to describe the fundamentals of friction of metals. According to the Prandtl−Tomlison model, friction forces arise from dissipation of elastic energy stored in the contact between single asperities by means of thermally activated local jumps from one surface potential energy minimum to another.[1] This model has been successfully applied to understand atomic stick−slip motion in nanoscale friction measurements on atomically smooth surfaces.[2,3] According to Bowden and Tabor, friction forces on metals arise from their resistance to plastic deformation of a sliding contact and can be separated in shearing forces and ploughing forces.[4] Both models have been developed for crystalline materials and do not consider chemical reactions between the contacting bodies. Chemical effects on the tribology of metals have mostly been investigated on the basis of tribo-induced formation of compacted surface oxides or glazes that have been reported to lower both friction coefficient and wear rate.[5]

Metallic glasses are multicomponent alloys consisting of at least two metallic elements or one metal, nonmetal, or metalloid, i.e., B, P, C, Si, or Ge, whose composition is selected to frustrate their crystallization upon cooling from the melt.[6] Metallic glasses are structurally amorphous. In contrast to crystalline metals, whose long-range order is only locally disturbed by the occurrence of defects, such as substitution or interstitial atoms, dislocations, and grain or phase boundaries, the structure of metallic glass is characterized by a random distribution of short and medium range ordered atomic clusters.[7] Consequently, the mechanisms for plastic deformation of crystalline and amorphous metallic materials are fundamentally different. In crystalline metals plastic deformation occurs by multiplication and motion of homogeneously distributed pre-existing dislocations. In metallic glasses plastic deformation is localized in narrow shear bands that propagate throughout a sample with high velocity, in the majority of cases leading to catastrophic failure without macroscopic tensile ductility, though some of BMGs exhibit remarkable damage tolerance and plasticity under compression.[8]

Similar to metals, the tribological behavior of metallic glasses has been reported to correlate with their hardness.[9] The tribology of metallic glasses has been discussed to be affected by structural relaxation, material transfer, and oxidation.[10−12] Most of the methods applied in these investigations did not allow for a clear identification of the mechanisms involved in the friction and wear of metallic glasses. In this respect, it remains necessary to investigate how structural properties affect the tribological behavior of metals.

Clean metallic surfaces are prone to surface alloying even at room temperature.[13] While the constitution and structure of surface alloys have been the subject of intensive research, the

Received: August 23, 2013
Accepted: October 21, 2013

dx.doi.org/10.1021/am403564a | ACS Appl. Mater. Interfaces XXXX, XXX, XXX−XXX

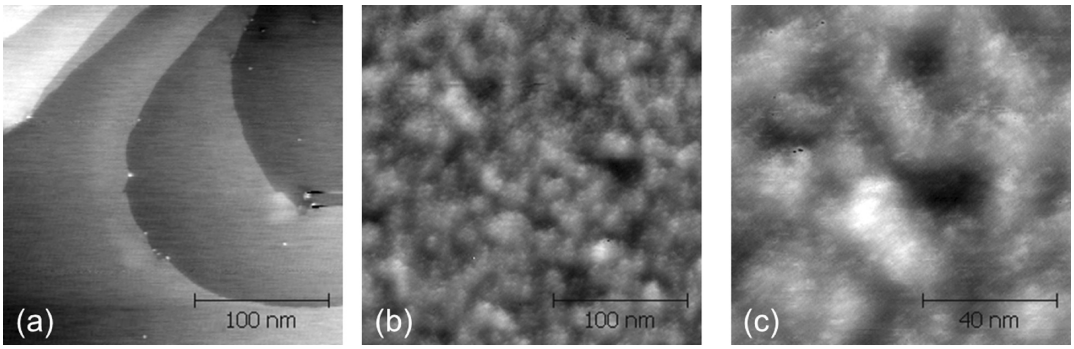

Figure 1. Noncontact AFM images recorded on (a) Pt(111) and (b, c) Pt-based metallic glassy ribbon. The z-range of the images is (a) Δz = 2.8 nm, (b) Δz = 1.9 nm, and (c) Δz = 1.3 nm.

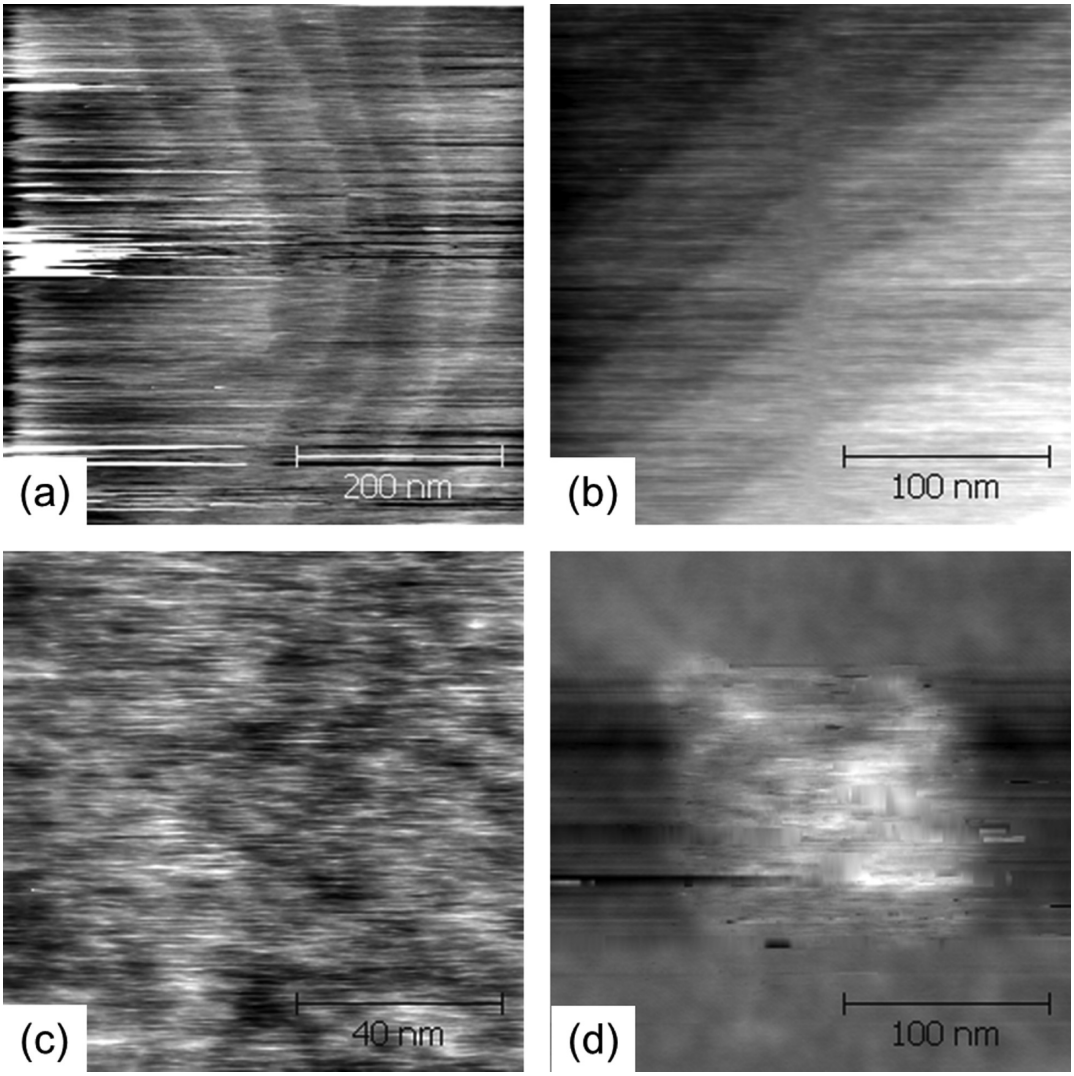

Figure 2. (a, b) Contact AFM topography images recorded on Pt(111) with (a) a SiO_x tip and (b) a diamond-coated tip. (c) Contact AFM topography image recorded on Pt-based metallic glass with a diamond tip and (d) subsequently recorded noncontact AFM topography image of the same area recorded with the same tip.

effect of surface alloying on the tribology of metals has not been investigated, though it may open new routes in the control of friction by selected alloying.

In this work, we determined the role of structure and chemistry for friction and wear of Pt-based metallic surfaces in sliding contact by atomic and friction force microscopy (AFM and FFM) and AFM-based scratching in ultrahigh vacuum. Clean Pt(111) and $Pt_{57.5}Cu_{14.7}Ni_{5.3}P_{22.5}$ (Pt-based) metallic glass surfaces were investigated with a SiO_x AFM tip and a diamond-coated AFM tip. This enabled us to separate the effects of structure and chemistry involved in single asperity sliding contact with reactive surfaces such as Pt-based metallic surfaces over a wide range of loads. We discuss our results on

dx.doi.org/10.1021/am403564a | ACS Appl. Mater. Interfaces XXXX, XXX, XXX−XXX

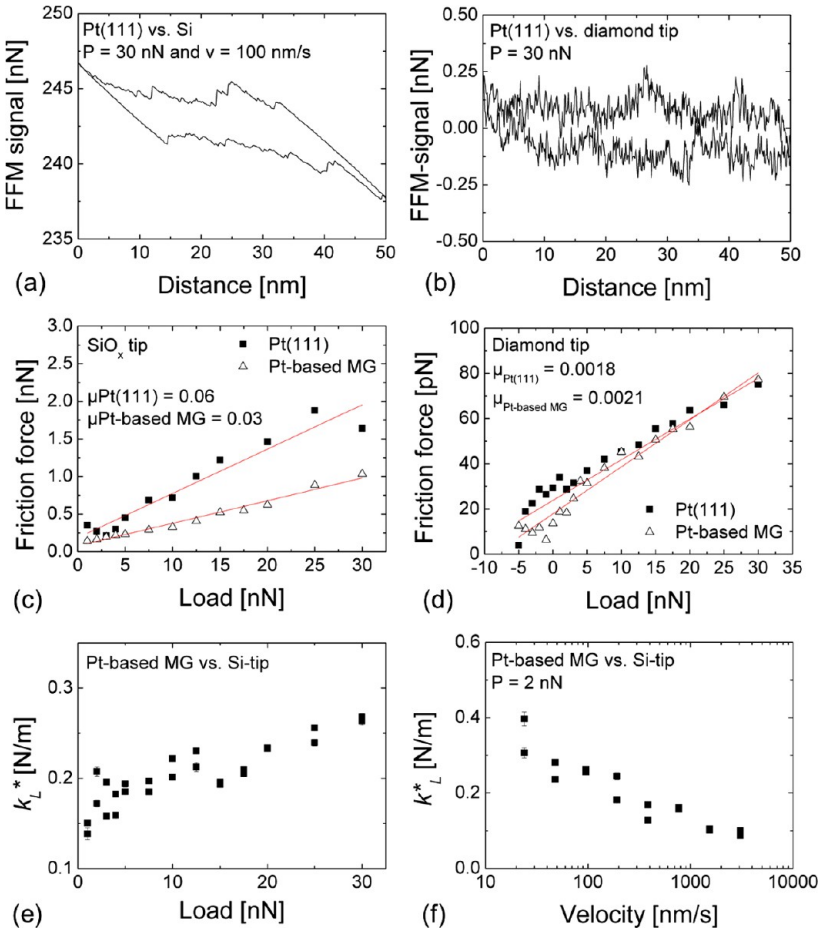

Figure 3. (a, b) Friction loops on Pt(111) recorded with (a) a SiO_x AFM tip and (b) a diamond AFM tip. (c, d) Load-dependent friction on Pt(111) and Pt-based MG with (c) a SiO_x tip and (d) a diamond-coated tip; (e) load and (f) velocity dependence of the lateral contact stiffness between the SiO_x tip and Pt-based metallic glass. In (c) and (d) the error in the friction force was determined from the instrumental noise as measured during an FFM measurement out of contact; we found the error in the friction force to be 10 pN.

the basis of interfacial alloying and plasticity involved in the sliding contact of an AFM tip with a smooth metallic surface.

II. SAMPLE PREPARATION AND EXPERIMENTAL METHOD

The surface of a Pt(111) single crystal (purchased from Mateck) was prepared by repeated cycles of Ar-ion sputtering with E = 1 keV for 20 min and thermal annealing at T_a = 1000 °C for 60 min to obtain an atomically smooth surface and characterized by low-energy electron diffraction (LEED) and Auger electron spectroscopy (AES). Figure 1(a) shows a typical noncontact (nc)-AFM topography image in which 100 nm wide atomically flat terraces are observed. After preparation of the Pt(111) surface LEED patterns displayed the typical 6-fold symmetry for (111) oriented fcc materials, while AES spectra confirmed the absence of contaminants such as C, H, S, and O. A $Pt_{57.5}Cu_{14.7}Ni_{5.3}P_{22.5}$ master alloy was prepared by prealloying P to Ni by induction melting in an evacuated quartz-glass tube and subsequent alloying of the remaining elements by arc melting in a Zr-gettered Ar atmosphere. The master alloy was then exposed to fluxing treatment with B_2O_3 and subsequently melt spun on a Cu wheel to produce 20 μm thick amorphous metallic ribbon samples with the above chemical composition. The amorphous structure of the Pt-based metallic glass was confirmed by X-ray diffraction (XRD) with K_α Cu radiation and differential scanning calorimetry (DSC) that revealed a broad diffraction peak at 39.866 degrees of 2θ and a clear glass transition at T_g = 223 °C and crystallization at T_x = 295 °C measured at 0.67 K/s. The surface of an as-spun Pt-based metallic glass ribbon was prepared by Ar sputtering with E = 1 keV for 5 min to remove its native oxide layer. After preparation the Pt-based metallic glass surface was characterized by AES that confirmed the absence of surface contaminants such as C, H, S, and O. Figure 1(b, c) shows typical nc-AFM topography images recorded on Pt-based metallic glass that reveal a random surface structure. Several characteristic length scales can be identified in Figure 1(b, c): we observe point-like structural units of several nanometers in size that agglomerate in *clouds*; on a broader scale these *cloud*-like agglomerates build ring structures of a few tens of nanometers in size. Surface characterization methods are promising in determining the structure of metallic glasses. Ashtekar et al. used STM at various temperatures to demonstrate the dynamics of spatial heterogeneities below the glass transition temperature of a metallic glass.[14] Oreshkin et al. investigated surface structural evolution of a NiNb metallic glass by STM and brought their observation with X-ray diffraction analysis to identify the local devitrification mechanisms.[15]

The friction and wear behavior of Pt-based metallic surfaces was investigated in ultrahigh vacuum by FFM using a VT-AFM manufactured by Omicron, Germany. The wearless friction behavior of Pt(111) and Pt-based metallic glass was determined in single asperity contact by sliding an AFM tip at the end of a soft micromanufactured cantilever beam perpendicularly to its length axis over the sample surface. In this work we used two different cantilevers on both Pt(111) and Pt-based metallic glass: a single crystalline Si AFM cantilever with a native SiO_x surface layer (Type: PPP-CONT, manufactured by NanoSensors) and a diamond-coated single crystalline Si AFM cantilever (Type: CDT-CONTR, manufactured by NanoSensors). In the following both cantilevers/tips will be referred to as SiO_x and diamond cantilever/tip, respectively. The

dx.doi.org/10.1021/am403564a | ACS Appl. Mater. Interfaces XXXX, XXX, XXX−XXX

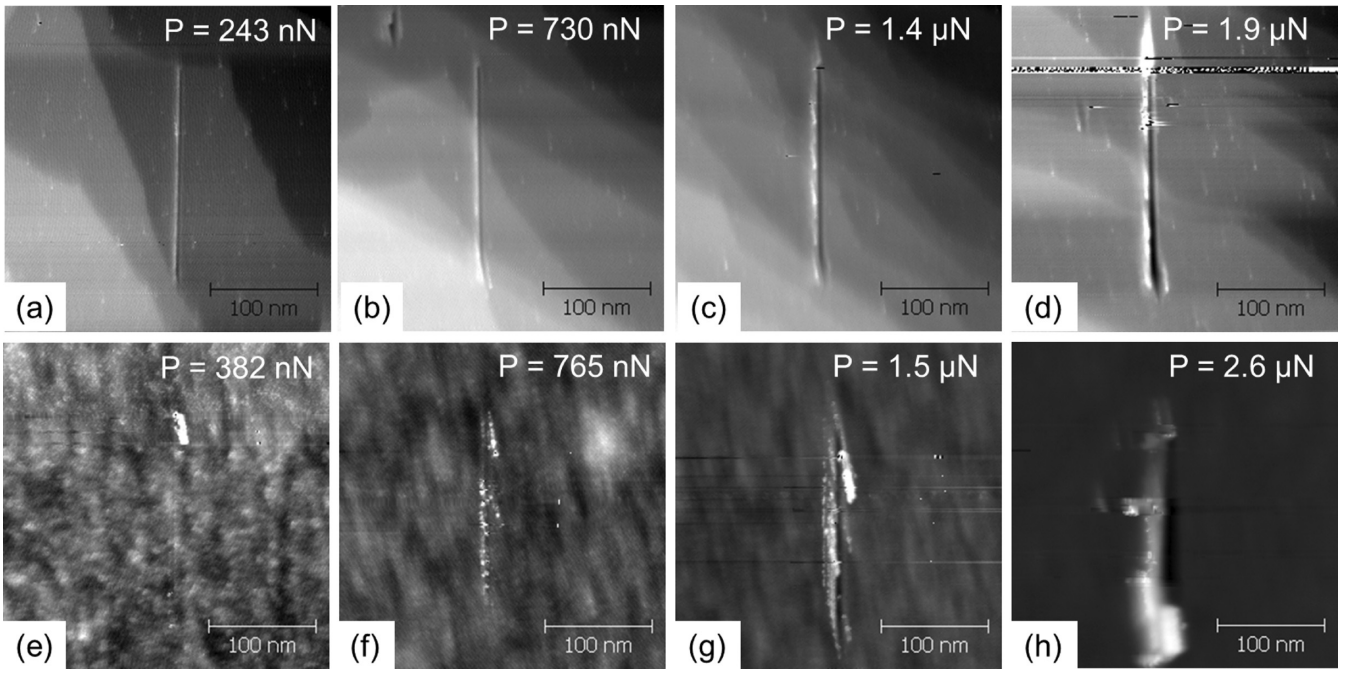

Figure 4. Noncontact AFM images of (a) Pt(111) and (b) Pt-based metallic glass after AFM-scratching tests at the indicated loads P and with v = 133 nm/s. (a–h) The image size is 300 × 300 nm^2. Single shear bands are indicated by an arrow. Note the granular appearance of plastically deformed material on metallic glass surfaces, which may indicate nanorecrystallization.

cantilevers' bending and torsion stiffness were calculated according to the beam geometry method.[16] We obtained k_n = 0.157 N/m and k_l = 80.735 N/m for the SiO_x cantilever and k_n = 0.31 N/m and k_l = 161.216 N/m for the diamond cantilever. Similarly, the wear behavior of Pt(111) and Pt-based metallic glass was investigated by reciprocal AFM-based scratching with a stiff diamond-coated single crystalline AFM cantilever (Type: DT-NCLR manufactured by NanoSensors) using the same experimental setup as above. The choice of a diamond-coated counter body was led by its mechanical stability over the series of experiments carried out in this work. Also diamond is chemically inert so that the results obtained from AFM scratching were expected to reflect the intrinsic wear properties of the samples under investigation. For this cantilever, the bending and torsional stiffness were determined as k_n = 53 N/m and k_l = 6778 N/m, respectively.

III. RESULTS AND DISCUSSION

The role of chemistry in the wearless regime is exemplified in Figure 2 for Pt(111) in contact with SiO_x and diamond AFM tips at similar loads, P = 2–5 nN. The contact AFM topography image recorded on Pt(111) with the SiO_x AFM tip reproduces the atomically flat terraces and their steps. However, it is clearly apparent that the sliding contact was affected by local sticking between a SiO_x AFM tip and Pt(111), as revealed in the friction loop in Figure 3. In the case of Pt(111) imaged with a diamond AFM tip, monatomic terraces and steps appear more clearly, though the steps are less sharp due to the larger tip apex. The friction loop corresponding to this tribological couple does not exhibit the sharp sticking events observed for a SiO_x AFM tip (see Figure 3). For both couples force distance curves have been recorded to determine the adhesion forces. For the contact between a SiO_x AFM tip and Pt(111), typical adhesion forces P_{ad} were in the range of 10–35 nN, for a diamond AFM tip in the range of 10–20 nN. In both cases, the adhesion forces were not influenced by the applied load or previous scanning. Figure 2 shows a contact AFM image of Pt-based metallic glass together with a noncontact AFM image subsequently recorded on the same area with a diamond tip. The area scanned in contact exhibits an elevated topography. This elevation cannot be explained by wear, in which case pile-ups at the edges of the area scanned in contact would be expected. The elevation rather indicates the wetting of the AFM tip and the formation of a moving contact neck. Figure 3 shows the load dependence of friction on Pt(111) and Pt-based metallic glass measured with a SiO_x AFM tip and a diamond AFM tip as counter bodies. In all cases we observed a linear increase of the friction force with increasing load. Consequently, we fitted our experimental data with a linear function whose slope corresponds to the friction coefficient μ. With a SiO_x AFM tip as a counter body, the friction coefficient was found to be $\mu_{Pt(111)/SiOx}$ = 0.06 and $\mu_{Pt\text{-based}/SiOx}$ = 0.03 for Pt(111) and Pt-based metallic glass, respectively. In contrast no significant difference in the friction coefficient of Pt(111) and Pt-based metallic glass was observed when measured with a chemically inert diamond AFM tip as a counter body; in both cases $\mu_{Pt(111),Pt\text{-based}/diamond} \approx 0.002$. For all series of friction measurements shown in Figure 3, an increase of the tip size was excluded by measuring the adhesion forces before and after each series of friction measurements. Significant changes of the tip shape were also excluded by reproducing the friction results for increasing and decreasing normal load. For the measurements with SiO_x AFM tips shown in Figure 2(c) the adhesion forces varied between 16 and 22 nN and for diamond AFM tips shown in Figure 2(d) between 13 and 17 nN. On the one hand, these results evidence the absence of structural effects on the wearless friction behavior of Pt-based metallic surfaces. On the other hand, the large difference in friction when measured with counter bodies of different chemistry strongly demonstrates the extent of chemical effects in wearless sliding contact with reactive Pt-based metallic surfaces. With a SiO_x AFM tip the friction coefficient on Pt(111) was twice as high as on Pt-based metallic glass. This difference can be attributed to the higher chemical reactivity of pure Pt than of its alloys and will be discussed below with regards to interfacial alloying. Also, we investigated

dx.doi.org/10.1021/am403564a | ACS Appl. Mater. Interfaces XXXX, XXX, XXX–XXX

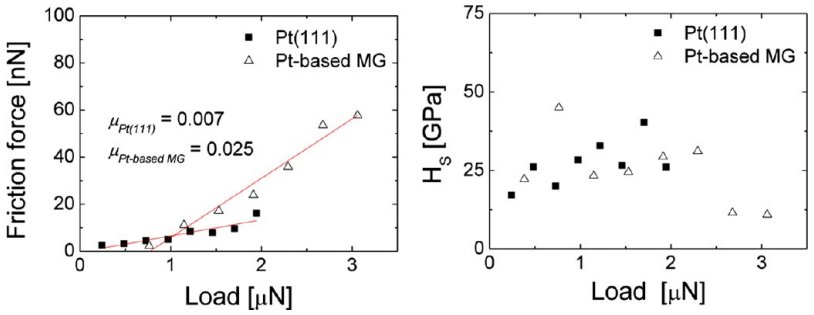

Figure 5. (Left) Load-dependent friction and (right) scratch hardness $H_S = P/A_c$ of Pt(111) and Pt-based metallic glass during AFM scratch experiments with a diamond-coated tip in ultrahigh vacuum. The contact area A_c was determined from the distance d between the summits of opposite pile-ups in the topographical cross section of the scratches in Figure 4. The contact area was assumed circular with a diameter d. The error in the friction force was determined from the instrumental noise as measured during a measurement out of contact; we found the error in the friction force to be 2 nN. The error in the scratch hardness was determined from the variation in the scratch width $\Delta d/d = 5\%$. For the error in the scratch hardness we found $\Delta H_s/H_s = 10\%$.

the velocity dependence of friction on Pt(111) and Pt-based metallic glass with a SiO_x AFM tip and diamond AFM tip (not shown here). In all cases friction was constant over the velocity range applied in this work (v = 20−2000 nm/s), which is in contrast to observations on Cu(111), where friction forces increased with the logarithm of the velocity in agreement with the Prandtl−Tomlinson model.[2]

In the case of Pt-based metallic glass we calculated the lateral stiffness k_L* of the contact with a SiO_x AFM tip as a function of the applied load and the sliding velocity (see Figure 3). According to Carpick et al. the contact lateral stiffness can be determined by measuring the slope of the FFM signal with regard to the sliding distance at the turning points of the sliding path.[17] Figure 3 shows the load and velocity dependence of k_L* for a SiO_x AFM tip in sliding contact with Pt-based metallic glass. We observe a sublinear increase of the lateral contact stiffness with increasing load. The obtained values k_L* = 0.15−0.27 N/m differ by 2 orders of magnitude from the published results on mica, k_L* ≈ 40 N/m.[17] According to the Hertz theory for elastic contact, k_L* = 8G*a, where a is the contact radius, $G^* = [(2 - \nu_t)/G_t + (2 - \nu_s)/G_s]^{-1}$, and $G_{t,s}$ and $\nu_{t,s}$ are the shear modulus and the Poisson's ratio of the tip and sample, respectively.[18] Given the higher elasticity moduli of Pt-based metallic glass ($G_{Pt\text{-based}}$ = 33.3 GPa and $\nu_{Pt\text{-based}}$ = 0.42) than the ones of mica (G_{mica} = 13.5 GPa and ν_{mica} = 0.10) a higher lateral contact stiffness could have been expected for Pt-based metallic glass than for mica.[19,20] The small values obtained for k_L* on Pt-based metallic glass can thus not be explained within the framework of elastic contact only but may reflect a liquefaction-induced softening of the contact. This is moreover infirmed by the decrease of k_L* with increasing sliding velocity that can be explained by a Newtonian flow within the sliding contact between a SiO_x AFM tip and Pt-based metallic glass.

We investigated the wear behavior of Pt(111) and Pt-based metallic glass in reciprocal sliding AFM scratch tests with a stiff diamond-coated AFM cantilever. Figure 4 shows nc-AFM topography images of scratches on (a−d) Pt(111) and (e−h) Pt-based metallic glass produced at the indicated loads ranging from 243 nN to 2.6 μN. In the case of Pt(111), wear already set on at a load P = 243 nN and occurred by homogeneous plastic deformation, i.e., ploughing of materials aside of the indenter. We observe a linear increase of the scratch width with increasing load and a monotonous increase of the pile-up along the scratches. In the case of Pt-based metallic glass, wear set on at a higher load P = 382 nN than on Pt(111). In this case plastic deformation was located in narrow shear bands (see Figure 4(f, g)). In the load range P = 382−2200 nN the scratch width increased linearly until a sudden increase was observed from P = 2.6 μN that coincides with the merging of isolated shear bands into a single shear zone along the scratch (see Figure 4(h)).

Friction forces were recorded during the scratch tests (see Figure 5). For both samples we observe a linear increase of the friction force with increasing load. Correspondingly the experimental data were fit with a linear function to calculate the friction coefficient. For Pt(111) we obtained $\mu_{Pt(111)}$ = 0.007 which is 3−4 times higher than in the wearless regime. For Pt-based metallic glass, $\mu_{Pt\text{-based}}$ = 0.025, i.e., one order of magnitude higher than in the wear-less regime. Similar results were reported by Park et al. for a Al−Ni−Co decagonal quasicrystal, and the increase of friction in the plastic deformation regime was attributed to bond formation and rupture within the contact junction between tip and substrate.[21] In their work the increase of friction was accompanied by an increase in adhesion, which may have arisen from the rupture of the aforedeposited passivating layer. It is interesting to note that the friction coefficient measured during wear on Pt-based metallic glass is 4 times higher than on Pt(111). Figure 5 also shows the load dependence of the scratch hardness H_S for Pt(111) and Pt-based metallic glass. In the load range P = 300−2000 nN we observe for both samples a linear increase of the scratch hardness from 20 to 38 GPa. In the case of Pt-based metallic glass H_S suddenly drops to 10 GPa at loads P > 2.6 μN, which coincides with the development of a single shear zone along the scratch in Figure 3(h) and corresponds to the shear softening of metallic glasses above yielding.[8]

In the wearless regime friction does not depend on the structural properties of the samples but strongly depends on the chemical composition of the counter body. On quasicrystals though Park et al. measured different friction forces depending on the crystallographic direction.[22] To this end the authors passivated either the surface or the AFM tip to avoid interfacial chemical reactions. The above results give strong evidence of chemical reaction at the interface between tips and samples (see Figures 2 and 3). The wetting of sharp indenters contacting metal surfaces has been previously observed in in situ indentation experiments by TEM.[23] There, a sharp Au-coated W tip was observed to form a neck with a Au(110) surface upon contacting. Upon retraction of the tip the neck was observed to undergo plastic liquid-like deformation, i.e., large

dx.doi.org/10.1021/am403564a | ACS Appl. Mater. Interfaces XXXX, XXX, XXX−XXX

elongation and thinning. Similar results were obtained by simulating the approach of a Ni tip toward a Au surface and its subsequent retraction.[24] After snap-in to contact the Au surface was observed to bulge under the Ni tip and to partially wet the tip. Again, the formation of a Au neck between the Ni tip and Au surface and the remaining of a Au adhesive layer on the Ni tip were observed upon separation. As discussed above, we believe that these mechanisms lead to the topographic elevation observed in Figure 2d.

For the present results we also attribute the velocity independence of friction to the formation of a neck between the tip and samples. Given the low k_L* values obtained with a diamond tip on Pt-based metallic glass and their decrease with increasing sliding velocity, we further argue that the neck between the tip and surface is of *liquid-like* nature and that the relative sliding of the tip on the sample was realized by the flowing of the neck acting as a lubricant. In this case, the measured friction forces were in the range of 1−100 pN and significantly lower than previously reported values on metallic surfaces under comparable loading conditions.[2] This picture further explains why structural differences between Pt(111) and Pt-based metallic glass do not cause any difference in their wearless friction behavior when measured with a diamond tip. The effect of the chemical composition of the counter bodies on the friction behavior of Pt(111) and Pt-based metallic glass can be explained by tribo-induced interfacial alloying. Though surface alloying of both miscible and immiscible metallic elements has been well documented in the case of room-temperature thin-layer deposition,[13] its effect on tribology has not yet been reported. Diamond is chemically inert and is thus not expected to react with Pt(111) and Pt-based metallic glass. In contrast, Si has a high affinity to Pt and tends to build silicides.[25] In the case of Pt thin films deposited on Si and subsequently annealed at 265 °C for 10 min, Ottaviani et al. observed the formation of Pt_2Si at the Pt/Si interface.[26] The affinity of Si to Pt can be described by the mixing enthalpy for Pt and Si of $\Delta H^{L}_{mix} = -72$ kJ/mol for a liquid alloy with 50 atom % Si.[27] The tendency for Pt−Si alloys to build Pt_2Si or PtSi phases can be described by their standard enthalpy of formation $\Delta H^{S}_{Pt_2Si} = -185$ kJ/mol and $\Delta H^{S}_{PtSi} = -118$ kJ/mol.[27] These thermodynamic quantities indicate the high reactivity of Pt and Si. In the case of a SiO_x AFM tip sliding on Pt(111) and Pt-based metallic glass, we attribute the increased friction compared to a diamond AFM tip to the alloying of Si with Pt in the neck formed between the tip and sample surface. In particular, the difference in friction between a SiO_x AFM tip and Pt(111) on the one hand and Pt-based metallic glass on the other hand reflects the different degree of reaction between Pt and Si and thus the availability of Pt to react with Si. In the case of Pt-based metallic glass, the Pt concentration is half of that in Pt(111); correspondingly, the friction coefficient on Pt(111) is twice as high as on Pt-based metallic when measured with a SiO_x AFM tip. It is interesting to compare our results with earlier results by Enachescu et al. on the friction of Pt(111) by UHV-AFM, where the authors used a WC-coated tip as the counter body.[3] The authors pointed at the high adhesion forces up to $P_{ad} = 1.2$ μN between a Pt(111) and a clean tip prepared by contact scanning under high load. For clean tips scanning at low force was accompanied by surface damage, and no atomic stick−slip could be observed. In contrast, measurements performed with a passivated tip regularly showed atomic stick−slip patterns. Higher adhesion forces than in the present study of *clean* WC-coated tips were explained by strong bond formation between the tip and sample. We attribute the difference in adhesion to differences in the chemical nature of the tip and in tip preparation. Enachescu prepared a clean WC-coated tip by prolonged scanning at high load, probably increasing the tip radius and thereby adhesion. In our work the sharp tips were prepared only by heating after introduction in UHV to remove adsorbents and may thus not exhibit strong reactivity.

Our results on wear show that wear mechanisms strongly depend on the structure of the investigated materials due to the different plasticity mechanisms. Wear of Pt(111) occurs by homogeneous plastic deformation, which is consistent with the delocalized character of dislocation-mediated deformation. The corresponding friction coefficient is 3 to 4 times higher than in the wearless regime when measured with a diamond AFM tip. We attribute this difference to the forces required to plough the material ahead of the tip in scratch experiments. The friction forces measured on Pt(111) during wear experiment with a diamond AFM tip are about 1 order of magnitude lower than reported by Mishra et al. in the case of Cu(100) at comparable loading forces: At $P = 250$ nN we measured a friction force $F_f = 5$ nN on Pt(111), while Mishra et al. measured $F_f = 30$ nN on Cu(100) at $P = 78$ nN.[28] We attribute this difference to the different crystallographic orientations of the investigated surfaces. Both Cu and Pt are fcc materials whose glide planes have {111}-orientation. For fcc metals, the activation of plastic deformation is easier on a (111) surface than on a (100) surface, thus giving rise to higher friction forces in the latter case than in the former one. In both cases of Pt(111) and Cu(100) nc-AFM imaging after scratching revealed the formation of similar pile-ups along the scratches.

In contrast, the wear of Pt-based metallic glass proceeded by localized plastic deformation as evident from the occurrence of shear bands along scratches. Above a critical load shear bands in Pt-based metallic glass merged into a single shear zone. At this load also we observed a sudden increase in the width of wear track that corresponds to the shear softening of metallic glasses above yielding.[8] A grainy structure within shear bands in Figure 3(f, g) may also indicate nanocrystallization during shear band propagation. Shear band propagation has been discussed to significantly increase the local temperature due to quasi-adiabatic relaxation of stored elastic energy.[29] Nanocrystallization of transfer films and within wear tracks of metallic glass has already been observed after macrotribological tests.[30] In this study, Kong et al. discussed nanocrystallization within the wear tracks of a metallic glass on the basis of the flash temperature. On the other hand, Bhushan and Nosonovsky have demonstrated that with a decrease of the contact size the temperature rise in the contact significantly decreases.[31] In our case the heat generation and subsequent nanocrystallization rather originate from the quasi-adiabatic release of elastic energy in shear bands than from friction. The friction coefficient measured during wear on Pt-based metallic glass was 4 times higher than on Pt(111). This difference can be explained by structural relaxation upon sliding of Pt-based MG as an additional dissipation mechanism of elastic energy. It is further interesting to consider the scratch hardness as an indicator to wear resistance. We observe a similar linear increase of the scratch hardness from 13 to 30 GPa in the load range $P = 250$−2200 nN. Above $P = 2.2$ μN and consistent with the shear softening of metallic glasses, we observe a sudden drop of the hardness. It is worth noting that though the

friction coefficients of Pt(111) and Pt-based metallic glass differ significantly in the wear regime their scratch hardnesses indicate a similar wear resistance over a wide range of loads. Beyond the resistance to plastic deformation friction forces may also arise from the release of elastic energy stored in a sliding contact. Recently, it was shown how cyclic loading of a Zr-based metallic glass well below yielding led to structural relaxation and partial crystallization of the glass.[32] Unlike crystalline materials, amorphous metallic alloys can accommodate elastic strain by local structural relaxation. This dissipation mechanism may explain the higher friction forces recorded during scratch tests on Pt-based metallic glass than on Pt(111), though the wear rate of both materials was similar.

IV. CONCLUSION

To summarize, we have shown that in the wearless regime friction on the Pt-based metallic surface depends on the chemical composition of the counter body and its reactivity with a metallic surface rather than on the crystallinity. This opens a new route in the control of friction with an impact on the development of self-lubricated mechanical devices and for the development of friction-induced bonding techniques. On the other hand, wear has been demonstrated to strongly depend on the structure and to reflect the different mechanisms of plastic deformation in crystalline and amorphous metallic materials.

AUTHOR INFORMATION

Corresponding Author

*E-mail: arnaud.caron@inm-gmbh.de.

Notes

The authors declare no competing financial interest.

ACKNOWLEDGMENTS

A.C. and R.B. thank Prof. E. Arzt for continuing support of the project. A.C. is grateful to Prof. M.W. Chen for financial support during his visit at WPI-AIMR, Tohoku University, Japan, and for critical discussion. Further, A.C. and D.V.L.-L. thank Prof. K.S. Nakayama from the WPI-Advanced Institute of Materials Research, Tohoku University, Japan, and Prof. A. Inoue from the Institute of Materials Research, Tohoku University, Japan, for critical discussion. The authors thank Dr. Wada from the Institute for Materials Research, Tohoku University, Japan, for his help in the Pt-based metallic glass sample preparation.

REFERENCES

(1) Tomlinson, G. A. *Philos. Mag.* **1929**, *7*, 905−939.
(2) Bennewitz, R.; Gyalog, T.; Guggisberg, M.; Bammerlin, M.; Meyer, E.; Güntherodt, H. J. *Phys. Rev. B* **1999**, *60* (R11), 301−304.
(3) Enachescu, M.; Carpick, R. W.; Ogletree, D. F.; Salmeron, M. *J. Appl. Phys.* **2004**, *95*, 7694−7700.
(4) Bowden, F. P.; Tabor, D. *The friction and lubrication of solids*; Oxford University Press: Oxford, U.K., 2008.
(5) Stott, F. H.; Wood, G. C. *Tribol. Int.* **1978**, *11*, 211−218.
(6) Inoue, A. *Acta Mater.* **2000**, *48*, 279−306.
(7) Cheng, Y. Q.; Ma, E. *Prog. Mater. Sci.* **2011**, *56*, 379−473.
(8) Trexler, M. M.; Thadhani, N. N. *Prog. Mater. Sci.* **2010**, *55*, 759−839 and references therein..
(9) Zhang, G. Q.; Li, X. Y.; Shao, M.; Wang, L. N.; Yang, J. L.; Gao, L. P.; Chen, L. Y.; Liu, C. X. *Mater. Sci. Eng., A* **2008**, *475*, 124−127.
(10) Boswell, P. G. *J. Mater. Sci.* **1979**, *14*, 1505−1507.
(11) Kishore, U. S.; Chandran, N.; Chattopadhyay, K. *Acta Metall.* **1987**, *35*, 1463−1473.
(12) Caron, A.; Sharma, P.; Shluger, A.; Fecht, H.-J.; Louzguine-Luzguin, D. V.; Inoue, A. *J. Appl. Phys.* **2011**, *109*, 083515-1−7.
(13) Pleth Nielsen, L.; Besenbacher, F.; Stensgaard, I.; Laegsgaard, E.; Engdahl, C.; Stoltze, P.; Jacobsen, K. W.; Norskov, J. K. *Phys. Rev. Lett.* **1993**, *71*, 754−757.
(14) Ashtekar, S.; Lyding, J.; Gruebele, M. *Phys. Rev. Lett.* **2012**, *109*, 166103-1−5.
(15) Oreshkin, A. I.; Mantsevich, V. N.; Savinov, S. V.; Oreshkin, S. I.; Panov, V. I.; Yavari, A. R.; Miracle, D. B.; Louzguine-Luzgin, D. V. *Acta Mater.* **2013**, *61*, 5216−5222.
(16) Nonnenmacher, M.; Greschner, J.; Wolter, O.; Kassing, R. *J. Vac. Sci. Technol., B* **1991**, *9*, 1358−1362.
(17) Carpick, R. W.; Ogletree, D. F.; Salmeron, M. *Appl. Phys. Lett.* **1997**, *70*, 1548−1550.
(18) Johnson, K. L. *Contact Mechanics*; University Press: Cambridge, U.K., 1987.
(19) Schroers, J.; Johnson, W. L. *Phys. Rev. Lett.* **2004**, *93*, 255506-1−4.
(20) McNeil, L. E.; Grimsditch, M. *J. Phys.: Condens. Matter* **1992**, *5*, 1681−1690.
(21) Park, J. Y.; Olgetree, D. F.; Salmeron, M.; Ribeiro, R. A.; Canfield, P. C.; Jenks, C. J.; Thiel, P. A. *Phys. Rev. B* **2005**, *71*, 144203-1−6.
(22) Park, J. Y.; Ogletree, D. F.; Salmeron, M.; Ribeiro, R. A.; Canfield, P. C.; Jenks, C. J.; Thiel, P. A. *Phys. Rev. B* **2006**, *74*, 024203-1−10.
(23) Merkle, A. P.; Marks, L. D. *Wear* **2008**, *256*, 1864−1869.
(24) Landman, U.; Luedtke, W. D.; Burnham, N. A.; Colton, R. J. *Science* **1990**, *248*, 454−461.
(25) Okamoto, H. *Desk Handbook: Phase Diagrams for Binary Alloys*; ASM International: U.S.A., 2000.
(26) Ottaviani, G.; Tu, K. N.; Mayer, J. W. *Phys. Rev. B* **1981**, *24*, 3354−3359.
(27) Topor, L.; Keppla, O. J. *Z. Metallkd.* **1986**, *77*, 65−71.
(28) Mishra, M.; Egberts, P.; Bennewitz, R.; Szlufarska, I. *Phys. Rev. B* **2012**, *86*, 045452-1−8.
(29) Wilde, G.; Rösner, H. *Appl. Phys. Lett.* **2011**, *98*, 251904-1−7.
(30) Kong, J.; Xiong, D.; Li, J.; Yuan, Q.; Tyagi, R. *Tribol. Lett.* **2009**, *35*, 151−158.
(31) Bhushan, B.; Nosonovsky, M. *Nanotechnology* **2004**, *15*, 749−761.
(32) Caron, A.; Kawashima, A.; Fecht, H.-J.; Louzguine-Luzguin, D. V.; Inoue, A. *Appl. Phys. Lett.* **2011**, *99*, 171907-1−3.